RESEARCH ARTICLE

Advancements in Amorphous Solid Dispersions to Improve Bioavailability

Development and Evaluation of Amorphous Solid Dispersion of Riluzole with PBPK Model to Simulate the Pharmacokinetic Profile

Kanchan Bharti[1] · Deepika Deepika[2,3] · Manish Kumar[1] · Abhishek Jha[1] · Manjit[1] · Akhilesh[1] · Vinod Tiwari[1] · Vikas Kumar[2,3,4] · Brahmeshwar Mishra[1]

Abstract

In the current work, screening of polymers viz. polyacrylic acid (PAA), polyvinyl pyrrolidone vinyl acetate (PVP VA), and hydroxypropyl methyl cellulose acetate succinate (HPMC AS) based on drug-polymer interaction and wetting property was done for the production of a stable amorphous solid dispersion (ASD) of a poorly water-soluble drug Riluzole (RLZ). PAA showed maximum interaction and wetting property hence, was selected for further studies. Solid state characterization studies confirmed the formation of ASD with PAA. Saturation solubility, dissolution profile, and *in vivo* pharmacokinetic data of the ASD formulation were generated in rats against its marketed tablet Rilutor. The RLZ:PAA ASD showed exponential enhancement in the dissolution of RLZ. Predicted and observed pharmacokinetic data in rats showed enhanced area under curve (AUC) and C_{max} in plasma and brain with respect to Rilutor. Furthermore, a physiologically based pharmacokinetic (PBPK) model of rats for Rilutor and RLZ ASD was developed and then extrapolated to humans where physiological parameters were changed along with a biochemical parameter. The partition coefficient was kept similar in both species. The model was used to predict different exposure scenarios, and the simulated data was compared with observed data points. The PBPK model simulated C_{max} and AUC was within two times the experimental data for plasma and brain. The C_{max} and AUC in the brain increased with ASD compared to Rilutor for humans showing its potential in improving its biopharmaceutical performance and hence enhanced therapeutic efficacy. The model can predict the RLZ concentration in multiple compartments including plasma and liver.

Keywords amorphous solid dispersion · dissolution · hepatotoxicity · physiologically based pharmacokinetic model · riluzole

Introduction

Owing to the advancements in combinatorial chemistry and high throughput screening, a large number of drug molecules are discovered with target specificity [1]. However, most of them found to have poor bioavailability due to high hydrophobicity. Highly hydrophobic drugs are poorly aqueous soluble that limits their absorption and thus bioavailability. Poor aqueous solubility is one of the major factors for most of lead compounds to fail in clinical studies despite their promising therapeutic effect. A high percentage of marketed drugs (about 40%) and products in R&D pipeline (over 90%) found to have solubility limited absorption responsible for poor drug bioavailability. Therefore, a variety of formulation techniques have been employed to address solubility issues of hydrophobic

✉ Brahmeshwar Mishra
  bmishrabhu@rediffmail.com

1 Department of Pharmaceutical Engineering and Technology, Indian Institute of Technology (Banaras Hindu University), Varanasi 221005, India

2 Environmental Engineering Laboratory, Departament d' Enginyeria Quimica, Universitat Rovira i Virgili, Tarragona, Catalonia, Spain

3 Pere Virgili Health Research Institute (IISPV), Hospital Universitari Sant Joan de Reus, Universitat Rovira I Virgili, Reus, Catalonia, Spain

4 German Federal Institute for Risk Assessment (BfR), Department of Pesticides Safety, Max-Dohrn-Str. 8-10, 10589 Berlin, Germany

drugs. Formulation of poorly aqueous soluble drug as amorphous solid dispersion (ASD) can significantly improve the solubility and dissolution rate of drug. ASD is a potential supersaturated drug delivery system which improve the pharmaceutical performance of hydrophobic drug by increasing its aqueous solubility and dissolution rate. ASD consists of active component homogeneously dispersed within an excipient matrix to give a single-phase binary amorphous system. The amorphous form of drug as a result of ASD preparation is responsible for apparent solubility and improved dissolution profile compared to its crystalline counterpart. This can be due to the fact that drug in amorphous state does not require much energy to break the crystal lattice, and get easily dissolve in aqueous solvent than crystalline drug. Additionally, ASD can aid in attaining a high supersaturation state that may result in increased flux across the membrane, henceforth improving drug bioavailability. The hydrophilic polymeric matrix of ASD is responsible for increased wettability of hydrophobic drug responsible for attaining high solubility and a supersaturated state [2, 3]. ASDs of pure drug are highly thermodynamically unstable and can undergo solution mediated phase separation in absence of stabilizers. Withholding the drug in its amorphous state is a challenging task hence the type and concentration of polymer as stabilizer is paramount [1]. The physicochemical properties of drug as well as polymer significantly impact the properties of resultant ASD.

RLZ is a poorly water-soluble drug and has neuroprotective and anti-excitatory action. It is the only US FDA–approved drug for amyotrophic lateral sclerosis (ALS) for oral route of administration [4]. The human dose RLZ is 100 mg/day (50 mg twice a day), which attenuates the disease progression including a favorable risk to benefit ratio [5–7]. Clinical trials (approximately 18 months) have shown that RLZ can extend the survival time by 2–3 months with a reduction in death rate by 43%. However, the major challenges associated with RLZ is low bioavailability leading to reduced on-site efficacy and high dose–related drug-induced liver injury (DILI), accompanied with increased alanine aminotransferase (ALT) and aspartate aminotransferase (AST) levels. Neutropenia is another condition for which healthcare providers have to be vigilant [8]. The RLZ has a mean absolute oral bioavailability of only 60% [9]. It has a low solubility of 0.3 mg/ml responsible for dissolution rate limited absorption and poor oral bioavailability [1, 10].

To overcome the RLZ associated problems, formulation of drug as ASD is proposed and a better understanding of pharmacokinetic (PK) is required which can be achieved by PBPK model. PBPK models are mathematical models which incorporate physiological and biochemical parameters to predict the concentration-time profiles in different organs.

They give an edge in estimating the PK profile of drug in its preclinical ADME study, estimating the drug exposure in a target organ dependent on physicochemical properties of ASD [11]. The development of a PBPK model of ASD consider the pharmacokinetic profile of RLZ administered as ASD for determining its safety and efficacy assessment.

The objective of present work was (i) screening of polymers for the preparation of ASD, (ii) development of RLZ ASD with selected polymer, (iii) conducting the animal experiments for obtaining PK profile for RLZ ASD and marketed formulation, and (iv) development of PBPK model in rat for determining possible pharmacokinetic parameters in human and thus evaluating the ASDs efficacy and toxicity in humans. The model validation was done by extracting the clinical data on humans from published literature.

Materials and Method

RLZ was generously provided by Alkem laboratories, Mumbai, India, as gift sample. PAA, PVP VA, and HPMC AS were received as a gift sample from Ashland, Mumbai, India. 5-Methoxypsoralen and dimethyl sulphoxide-d6 were purchased from Sigma Aldrich. Pepsin, lecithin, and sodium taurocholate were purchased from SRL Pvt Lt. All the solvents used were of analytical grade.

Screening of Polymers

Preparation of Amorphous Solid Dispersion of RLZ

ASD was prepared employing rapid solvent evaporation technique in a rotary evaporator (IKA RV 10 auto pro V). 1:1 ratio of methanol and dichloromethane were taken for dissolving RLZ and PAA, PVP VA, and HPMC AS in different weight ratios (30:70, 20:80, and 10:90) under constant stirring. The prepared solution was then evaporated under vacuum at a bath temperature of 40°C, and a vacuum gradient of 500 mBar to 2 mBar was gradually applied. The ASDs were kept in a vacuum oven for 24 h at 25°C in order to eliminate remaining solvent. The samples were passed through ASTM #100 and stored at 4°C.

Nuclear Magnetic Resonance

The molecular level interaction in solution state was deciphered by performing ^{1}H-NMR (500 MHz) using Bruker 500 FT NMR spectrometer. The NMR spectra of RLZ, polymers, and physical mixtures of 70:30% w/w of drug and individual polymers were taken. All the samples were dried to remove moisture and then dissolved in dimethyl sulfoxide-d6. The values of chemical shifts have been reported in parts per million (ppm) which are referenced to internal standard

tetramethylsilane (TMS). The values of coupling constants (J) have been reported in hertz.

Contact Angle Study

For contact angle study, 150 mg of each powder sample (ASDs with different polymers in 10:90 drug polymer ratio, pure polymers, and pure drug) was compressed under hydraulic press for a dwell time of 30 s at a pressure of 50 MPa to form a cylindrical pellet with a 10-mm diameter. The contact angle of powder compacts was determined utilizing the Drop Shape Analyzer device (contact angle goniometer assembled by DuraVision) using the sessile drop method. A predetermined volume of water from a syringe was dispensed on the sample surface, and then, video images were captured. All the readings were taken in triplicate, and mean values are reported. The readings were taken under ambient condition.

Solid-State Characterization

Powder X-ray Diffraction Study

PXRD study of different ratio of RLZ:PAA ASD was evaluated under Rigaku Miniflex 600 X-ray diffractometer at ambient temperature. Monochromatic Cu K radiation at 100 mA and 40 kV in the vicinity of 5–50° scanned at 5°/min with an angular increase of 0.02°/s were used for the study.

Differential Scanning Calorimetry Study

To examine the thermal behavior of the prepared ASD, the samples were analyzed under DSC. Sample weighing approximately 3–5 mg was taken in crimped aluminum pans and heated under DSC from $-40—140°C$ at a scan rate of 20°C/min. Nitrogen purge at a rate of 50 ml/min was maintained throughout the DSC runs.

Transmission Electron Microscopy

For TEM studies, homogenous solutions of different ratio of drug and polymer in the 1:1 DCM: methanol mixture were prepared, and spin coated on 200 mesh carbon coated copper grid. Bright field images and selected area electron diffraction (SAED) pattern were captured on Tecnai G2T20 TEM operating at 200 kV for analyzing the samples.

High-Performance Liquid Chromatography Method

For quantitative analysis of drug in various studies a HPLC system (Waters Milliford, USA) connected to a photodiode array (PDA) detector (model 2998, Waters, USA),a LC system consisting of a binary pump (model 1525; Waters, USA), a manual injector valve with 20 μL loop, and C18 column (150 mm × 4 mm; 5 μm) was utilized. The injection volume of 20 μL was taken, and sample detection was done at a wavelength of 264 nm. The mobile phase constituted acetonitrile: water in a ratio of 65:35 and 1 ml/min flow rate. The analysis run time was 10 min. The Breeze program was utilized to carry out the data acquisition.

Biopharmaceutical Performance Evaluation

Saturation Solubility Study

The solubility of RLZ in different media was evaluated using the shake flask method. Media with different pH (1.2, and 6.8) and biorelevant media viz. fasted simulated gastric fluid (FaSSGF) and fasted simulated intestinal fluid (FaSSIF) were used for the study. The solubility study was done using shake flask method for 72 h at $37 \pm 0.5°C$. In a 100-ml volumetric flask, 50 mL of the media and about 100 mg of RLZ were added. After 24, 48, and 72 h, samples were taken out, filtered through 0.2 μm filters, diluted appropriately, and then subjected to an HPLC analysis. The study was done in triplicate, and mean values are reported.

In Vitro Dissolution Testing

The dissolution of RLZ from ASD *versus* Rilutor was evaluated employing USP type-II apparatus (Electrolab India Pvt Ltd.). Nine hundred milliliters of 0.1 N HCl (pH 1.2) and FaSSGF were used for the dissolution experiments, which were carried out at $37.0 \pm 0.5°C$ with a paddle rotating at a speed of 50 rpm. Rilutor tablets and RLZ ASDs equivalent to 50 mg RLZ were filled inside hard gelatin capsules and added to each vessel. Samples (5 mL) were taken at set intervals (5, 15, 30, 45, 60, 90, and 120 min). The volume was kept constant by adding fresh media in an equal amount. HPLC method as described above was used for the RLZ concentration determination. The study was done in triplicate, and mean values are reported.

Plasma and Brain Pharmacokinetics in Male Rats

The study was done according to the approved study protocol (IIT(BHU)/IAEC/2022/010). Adult male Wistar rats were kept in standard laboratory conditions and were provided with a standard pellet meal and water. Eight rats were divided randomly in two groups. The first group received RLZ-PAA ASD, while the second group received crushed Rilutor of RLZ at a dose equivalent to 10 mg/kg, administered orally via oral gavage. Before administration, each formulation was prepared by suspending it in a 0.5% w/w solution of carboxymethyl cellulose. Blood samples

were collected from the retro-orbital route at specific time intervals: 0, 0.25, 0.5, 1, 2, 3, 6, and 12 h, in heparinized micro-centrifuge tubes. Immediately after blood collection, plasma separation was done using a centrifuge at 7000 rpm for 5 min at 4°C. The supernatant plasma was separated using a micropipette and stored at − 20°C until further processing.

To study brain kinetics, thirty rats were divided into two groups. Each rat received an oral dose equivalent to 10 mg/kg RLZ-PAA ASD and crushed Rilutor of RLZ. Three animals each at 0.5, 1, 2, 6, and 12 h were killed for brain extraction. For brain homogenate preparation, the brain was weighed accurately and homogenized with 1:5 w/v of 50% v/v aqueous acetonitrile. The brain tissue sample was then centrifuged at 10,000 rpm for 10 min, and the supernatant was collected [10]. Samples of brain homogenate were stored at − 80°C until further analysis. The control blank plasma and brain were drawn from rats before dosing, processed, and stored until analysis.

For the preparation of the calibration curve, 90 μl of a biological sample (plasma or brain homogenate) was spiked with 10 μl of working solutions ultimately producing a drug concentration ranging from 20 to 2000 ng/ml [12]. The biological sample (100 μl) was taken, and ACN (100 μl) was added to facilitate protein precipitation. The mixture was vortexed for 1 min and then centrifuged at 10,000 rpm for 10 min. Supernatant (100 μl) was collected and subjected to heating at 80°C under constant nitrogen purge. The residue was then reconstituted with 100 μl solution of 5-methoxypsoralen in a concentration of 20 μg/ml and vortexed further for 5 min. The resultant solution was then injected into HPLC for drug quantification set at the parameter described above.

Literature Data Extraction for PBPK Modeling

Rat Literature Experimental Data

Data were extracted from a study by Ravi *et al*. where an oral dose of 10 mg/kg BW was administered to male Wistar rats weighing 180–220 g [13]. Plasma samples were analyzed at 0.25, 0.5, 1, 2, 3, 4, 6, 8, 12, and 16 h post dose and analyzed using HPLC method. Webplot digitizer was used for extracting the data for all literature studies [14].

Human Literature Experimental Data

To check PBPK model predictions, the clinical data done on humans were extracted from different literature. There were three independent studies in the literature where RLZ tablet formulation was administered to the human population and plasma samples were quantified. The first study was from Liboux *et al*. where 100 mg oral dose was given,

and plasma samples were quantified at various time points [15]. Another study was from Chandu *et al*. where a tablet of 50 mg was given to 54 healthy volunteers with 240 ml of drinking water. Blood samples were collected, and plasma was analyzed by LC-ESI-MS/MS [16]. The third study was taken from Longo *et al*. where 50 mg RLZ tablet during phase I study were administered and plasma concentration for 24 h were quantified [17].

Development and Optimization of the PBPK Model

Perfusion-limited PBPK model with 9 compartments viz., stomach, gut, liver, brain, kidney, lungs, fat, heart, rest body, and plasma, were developed considering Rilutor and ASD formulation (Fig. 1). The exchange of drug between blood and tissue in each organ is governed by blood flow also called as perfusion limited or flow limited model. The model was developed in rats due to availability of literature and in-house data and later extrapolated to humans which can be helpful in guiding clinical studies. Oral dosing was considered through gut using first-order rate constant. The unbound or free fraction (fu) was considered available for distribution, metabolism, and excretion from the body.

Distribution of drug from one compartment to another was controlled by partition coefficient along with blood flow. The partition coefficient of RLZ was taken from literature (wherever data available) for specific organs, and for remaining organs with no data availability, QSAR (quantitative structure activity relationship) model was used. Partition coefficient was calculated using Rodger and Rowland approach for perfusion-limited model [18]. The R script for Rodger and Rowland approach has been provided on GITHUB for users and also can be referred through the published literature [19]. The elimination of the drug was through metabolism in liver and excretion using urine and feces from the kidney and gut, respectively. There are six major and multiple minor metabolites of RLZ which are mostly metabolized in liver by hydroxylation and glucuronidation catalyzed by cytochrome P450 enzyme [20]. Among all metabolizing enzymes, CYP1A2 is majorly involved in riluzole clearance followed by UGT1A1. The major metabolite, N-hydroxy RLZ (RLZ-OH), generated with CYP1A2 enzyme was considered for this study. RLZ metabolism was described through Michaelis-Menten kinetics with parameters like V_{max} and k_m using the following equation.

$$V_{met} = \frac{V_{max} * C_{liver} * f_u}{K_m + C_{liver} * f_u} \tag{1}$$

The absorption parameters like gastric emptying, absorption rate constant, and bile rate constant were optimized based on experimental data. Fraction unbound (fu) was extracted from literature [20]. Renal clearance was taken
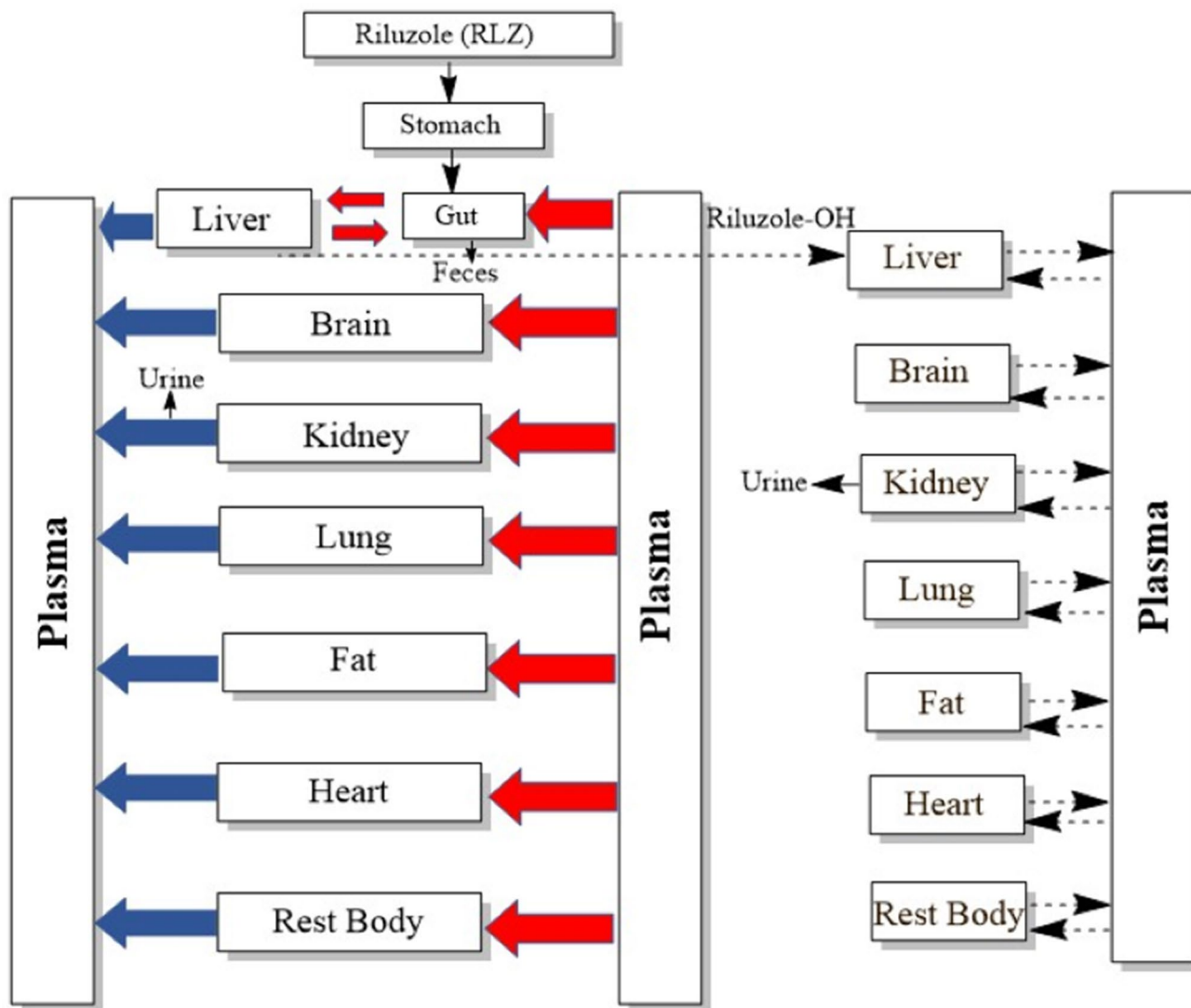
Fig. 1 Nine compartment PBPK model with excretion from urine and feces. The model was used to predict concentration-time profile in different compartments. RLZ-OH is being represented by dotted lines

from Longo *et al*. [17] where it was calculated by data extracted from Liboux *et al*. [15]. Fecal elimination was optimized considering 90% absorption in human [17]. The *in vivo* data by Ravi *et al*. was used for optimization of the parameters for the tablet formulation. Complete optimization details are provided in the supplementary file. In case of ASD, only three parameters which mainly reflect the biopharmaceutical component were changed (i.e., gut absorption rate constant, undissolved drug in feces, and bile rate constant). The detailed equation for PBPK has been provided in the supplementary file.

The model developed for rats of Rilutor and ASD was extrapolated to humans without any variation in the model structure. The rat physiological parameters were replaced with human-specific parameters. For the biochemical parameters, the highly accepted allometric scaling based on body weight was used (provided in Eq. 2) [21]. In Eq. 2, param refers to biochemical parameters which were scaled, and AE to allometric exponential value. Finally, a PBPK model for human was developed by adjusting the gastric emptying rate (GE) and keeping rest parameters similar. Different dosing scenarios at 50 and 100 mg were used for checking the prediction of the model with the observed data. The input parameters, i.e., physiological and biochemical, are provided in Table I.

$$\text{Param} = \text{Param} * \left(\frac{\text{BW\_human}}{\text{BW\_rat}}\right)^{\text{AE}} \qquad (2)$$

Table I Physiological and Biochemical Parameters Used for Rat and Human PBPK Model

Parameters	Value in rat for Rilutor, ASD	Reference
Blood flow to organ (fraction of cardiac output)		
Liver	0.174	[22]
Lung	0.021	[23]
Kidney	0.141	[24]
Heart	0.051	[21]
Brain	0.02	[21]
Fat	0.07	[25]
Volume of organ (fraction of BW)		
Liver	0.036	[24, 25],
Lung	0.006	[24]
Kidney	0.0073	[25, 26]
Heart	0.004	[26]
Brain	0.006	[24, 25]
Fat	0.07	[25]
Plasma	0.074	[25]
Biochemical parameters		
Liver:plasma	2.2	Taken from literature[a]
Brain:plasma	2.44	Experimental[b]
Kidney:plasma	4.622509	Calculated using R&R[e]
Lung:plasma	5.958539	Calculated using R&R[e]
Fat:plasma	14.12276	Calculated using R&R[e]
Heart:plasma	4.251126	Calculated using R&R[e]
GE ($1/h/kg^{0.25}$)	2.61	Optimized*
Kabs ($1/h/kg^{0.25}$)	0.69, 2.19	Optimized*
Fu (unitless)	0.04	Experimental[c]
FuM1 (unitless)	0.04	Considered similar as parent compound
V_{max} ($nmol/h/kg^{0.75}$)	250,000	Optimized*
K_m ($\mu mol/l$)	140	Optimized*
Clurine ($\mu l/h/kg^{0.25}$)	0.3771	Taken from literature[d]
ClM1urine ($\mu l/h/kg^{0.25}$)	0.3771	Considered similar as parent compound
Kfeces ($1/h/kg^{0.25}$)	0.013, 0.011	Optimized*
Blood flow to organ (fraction)		
Liver	0.257	[27]
Lung	0.034	[26]
Kidney	0.177	[27]
Heart	0.09	[28]
Brain	0.117	[23]
Fat	0.052	[27]
Volume of organ (fraction)		
Liver	0.026	[24, 27]
Lung	0.014	[24, 29]
Kidney	0.004	[24]
Heart	0.012	[28]
Brain	0.021	[24, 26]
Fat	0.187	[24]
Plasma	0.03976	[23]
Biochemical parameters		
Liver:plasma	2.2	Similar to rat
Brain:plasma	2.44	Similar to rat
Kidney:plasma	4.622509	Similar to rat

Table I (continued)

Parameters	Value in rat for Rilutor, ASD	Reference
Lung:plasma	5.958539	Similar to rat
Fat:plasma	14.12276	Similar to rat
Heart:plasma	4.251126	Similar to rat
GE (1/h/kg$^{0.25}$)	2.61	Optimized*
Kabs (1/h/kg$^{0.25}$)	0.69, 2.19	Similar to rat
Fu (unitless)	0.04	Similar to rat
FuM1 (unitless)	0.04	Considered similar as parent compound
V_{max} (nmol/h/kg$^{0.75}$)	250,000	Similar to rat
K_m (μmol/l)	140	Similar to rat
Clurine (μl/h/kg$^{0.25}$)	0.3771	Similar to rat
ClM1urine (μl/h/kg$^{0.25}$)	0.3771	Considered similar as parent compound
Kfeces (1/h/kg$^{0.25}$)	0.013, 0.011	Similar to rat

PBPK physiologically based pharmacokinetic, *RLZ* riluzole

[a]Longo *et al*. reported liver:blood partition coefficient of 2.0, with RLZ blood to plasma ratio of 1.1. Hence, liver:plasma partition was considered 2.2[17]

[b]Calculated using AUC brain from mice study at 10 mg/kg[30]

[c][20]

[d][17]. Author calculated renal clearance using data from Liboux *et al*. [15]

[e][18]

*Optimized based on experimental data from Ravi *et al*. [13] in Rilutor and for ASD using our in-house data for rat. For human, data from Liboux *et al*. [15] was used to optimize gastric emptying

Model Evaluation and Local Sensitivity Analysis

To evaluate the accuracy of the developed model predictions, a calibrated rat model using both our in-house *in vivo* data and rat data obtained from Ravi *et al*. was used. By comparing the plasma and brain concentration-time profiles generated by our model with the observed data, the model's predictive capabilities were accessed for Rilutor and ASD. PBPK model in humans was evaluated with data from multiple case studies [15–17]. The PK parameters were calculated and compared for both simulated and observed data. Furthermore, the predictions were made for ASD formulation in humans to evaluate the PK profile in plasma and brain.

A normalized local sensitivity analysis was performed to investigate the influence of biochemical model parameter on the output of the model (Eq. 3) [27]. Each parameter was increased by 1% to evaluate the change in plasma AUC. In Eq. 3, NSC stands for normalized sensitivity coefficient, inc refers to increase in AUC or parameter value, and ori refers to original value for the AUC or parameter.

$$\text{NSC} = \frac{(\text{AUC}_{inc} - \text{AUC}_{ori})/\text{AUC}_{ori}}{(\text{Param}_{inc} - \text{Param}_{ori})/\text{Param}_{ori}} \quad (3)$$

Ordinary differential equations (ODE) were used to develop the PBPK model which describes the PK of RLZ.

The equations were written in GNU MCSIM (Version 6.1.0) and solved by integration with Rstudio (Version 4.2.1). All the equations have been provided in supplementary file. Monte Carlo simulation was performed with 20,000 iterations along with the uncertainty in biochemical parameters to simulate the impact on model predictions.

Results

Screening of Polymers

Nuclear Magnetic Resonance

Figure 2 shows the overlay spectra of proton (^{1}H) NMR of the three physical mixtures and pure RLZ. The up-field shifts of NH$_2$ proton at 7.64 ppm was observed in all three physical mixtures. The maximum relative shift could be seen from 7.74 to 7.62 ppm in case of RLZ:PAA (green colored peak). The doublet peak of aromatic hydrogen of RLZ appearing at 7.37–7.35 ppm was flattened in the physical mixture.

Contact Angle Study

The static contact angle of the water with the surface of various polymers, ASDs, and RLZ was measured and displayed in Table II. Poorer wetting is associated with higher surface
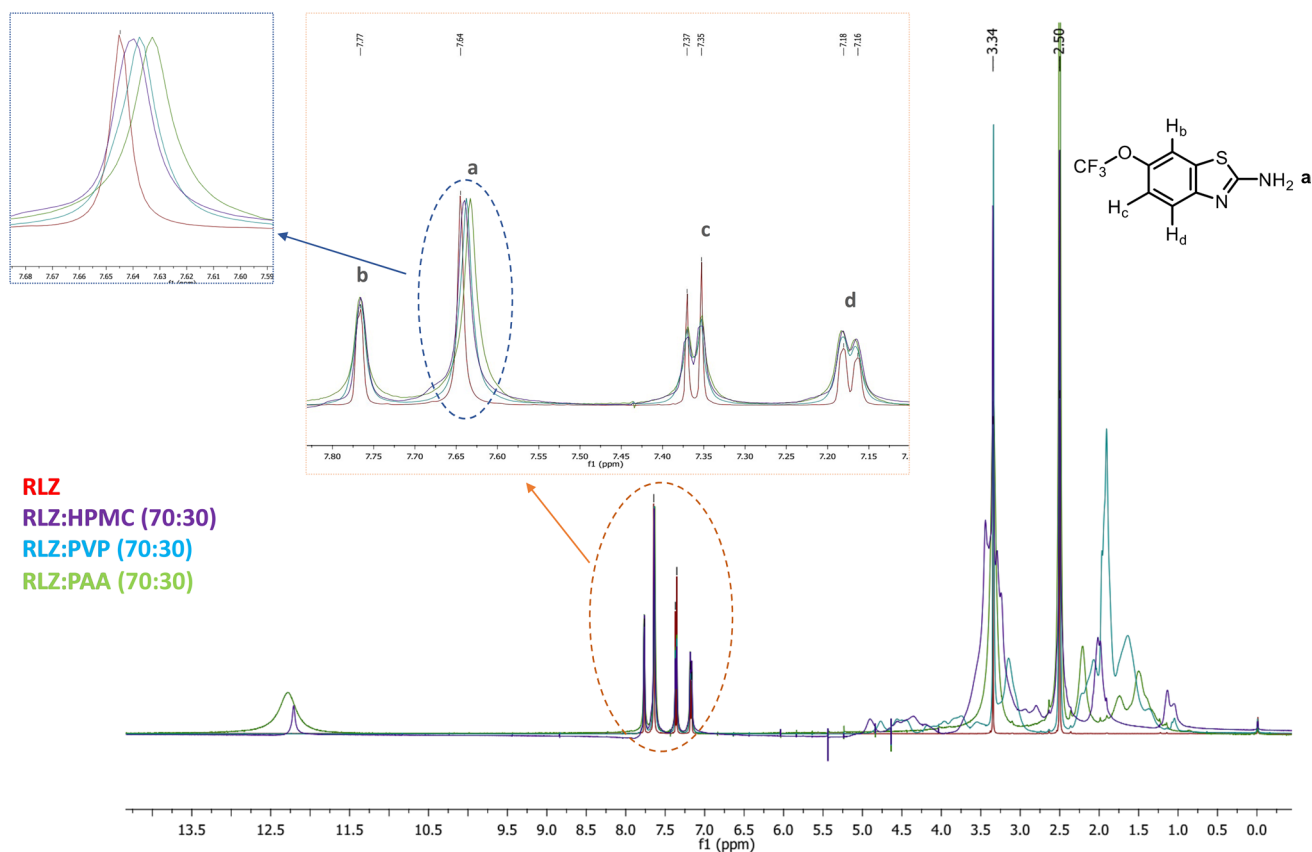
Fig. 2 Overlay of 1H NMR spectra of RLZ and its physical mixtures with each polymer in solution state, showing the change in the chemical shifts due to non-bonding interactions

hydrophobicity and is indicated by a higher contact angle value, and vice versa [31]. ASDs prepared with different polymers are ranked from most hydrophobic to least hydrophobic as follows: RLZ:PAA > RLZ:PVPVA > RLZ:HPMC AS. The pattern of polymer suitability obtained from this study is in reasonable agreement with the results obtained in the NMR study.

Table II Contact Angle of Water on Pure Drug, Polymers, and Prepared ASDs

S. no	Components	Contact angle (°)
1	RLZ	66.9 ± 3.1
2	PAA	33.4 ± 0.8
3	PVP VA	46.7 ± 1.9
4	HPMC AS	57.8 ± 1.4
5	RLZ:PAA ASD	29.3 ± 1.8
6	RLZ:PVP VA ASD	34.1 ± 2.7
7	RLZ:HPMC AS ASD	39.8 ± 2.2

ASD amorphous solid dispersion, *RLZ* riluzole, *PAA* polyacrylic acid, *PVP VA* polyvinyl pyrrolidone vinyl acetate, *HPMC AS* hydroxypropyl methyl cellulose acetate succinate,

Solid-State Characterization

Powder X-ray Diffraction Study

It is a widely used technique to determine the composition of the sample and the crystal structure. As seen in Fig. 3a, the pure crystalline form of RLZ showed sharp and distinct peaks at 2θ values of 9.14, 13.64°, 18.18°, 22.74°, and 25.22° demonstrating the crystalline nature of RLZ. However, the ASD of RLZ prepared with all the aforementioned ratios viz. 10:90, 20:80, and 30:70 RLZ: PAA ASD showed a complete absence of Bragg peaks.

Differential Scanning Calorimetry Study

DSC is a thermal technique that explains the physical properties of the drug molecule and the prepared formulations. In Fig. 3b, the DSC thermogram of pure crystalline RLZ and ASD prepared with different drug and polymer ratios viz. 10:90, 20:80, and 30:70 RLZ: PAA ASD are shown. The sharp endothermic peak occurring at 120°C corresponds to the melting point of RLZ hence demonstrating the crystalline nature of RLZ [32]. The other thermograms of the
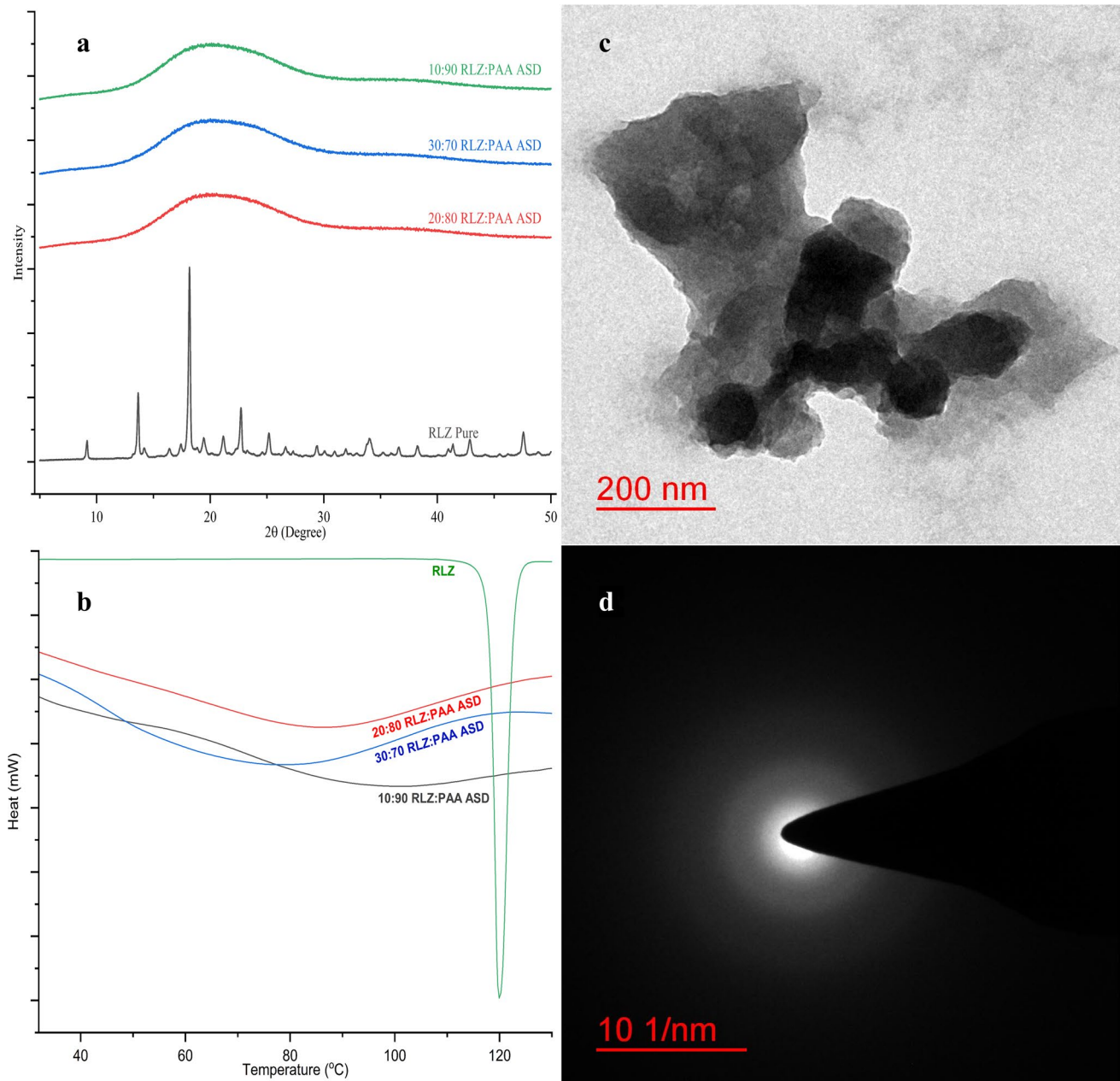
Fig. 3 **a** XRD plot of ASD prepared with different ratio of RLZ and PAA in comparison with pure crystalline RLZ. **b** DSC thermogram of RLZ, and RLZ: PAA ASD prepared with different drug and poly-mer ratio. **c** TEM image of the optimized ASD formulation. **d** SAED pattern of the optimized ASD formulation

prepared ASDs show the absence of sharp endothermic peaks; this is a clear indication of the amorphization of the drug. Hence, the successful preparation of the ASDs of RLZ with PAA is confirmed.

Transmission Electron Microscopy

The bright field images from multiple areas of the prepared sample were captured, as shown in Fig. 3c. The likelihood of forming any crystalline phase is very less as the morphology of the particle dictates to be spherical in the image. The SAED pattern (Fig. 3d) of the captured region exhibited diffused rings and complete absence of any systematic spot or array.

Biopharmaceutical Performance Evaluation

Saturation Solubility Study

RLZ is a fluorine containing weakly basic compound with a dissociation constant of 3.47. The solubility was observed

to be pH-dependent as it showed solubility of 12.43 mg/ml at acidic pH of 1.2 and very low solubility of 0.33 mg/ml at pH 6.8. The solubility of RLZ in FaSSGF and FaSSIF was slightly higher than pH 1.2 and pH 6.8, respectively. Hence, RLZ demonstrated higher solubility at pH 1.2 than pH 6.8. The solubility data of RLZ in different media is shown in Figure S1.

In Vitro Dissolution Testing

Figure 4a and b show the dissolution profile of the marketed tablet of RLZ, i.e., Rilutor and ASD RLZ: PAA in different ratio 30:70, 20:80, and 10:90. As seen in the dissolution profile at pH 1.2 in the initial 30 min, all the ASD formulations showed 100% drug release, while Rilutor showed 68% drug release. All the ASD formulations showed their maximum release of drug, and the profile became superimposable from the initial 60 min of the dissolution except for Rilutor. Additionally, model-independent similarity factor (f_2) of 35, 29, and 23, for 30:70, 20:80, and 10:90 RLZ:PAA ASD, respectively, give evidence of dissimilarity in the dissolution profile of ASD formulations with respect to Rilutor. Dissolution profile of Rilutor in FaSSGF was 75% after 60 min, and complete release was observed at 120 min of dissolution study. In FaSSGF RLZ:PAA 10:90, ASD showed complete release after 45 min, while RLZ:PAA 20:80 ASD and RLZ:PAA 30:70 ASD showed complete release after 60 min. Calculated f_2 value of 43, 38, and 33 for 30:70, 20:80, and 10:90 RLZ:PAA ASD, respectively, with respect to Rilutor, proves the difference in their dissolution profile.

Rat PBPK Model

Plasma and Brain Concentration for Rilutor

Rat PBPK model was used for the simulation of the single dose of 10 mg/kg BW/day after oral administration. Figure 5 shows a simulated plasma concentration-time profile for 24 h with blue line, black line, and red line representing percentile 2.5, median, and 97.5, respectively, along with experimental data in red circle from Ravi *et al*. [13]. It can be seen that the simulated details are quite close to the observed data at all time points. Figure 6 shows the plasma and brain profile at 10 mg/kg BW/day of our in-house data. Simulated data is within the range of 1.5–twofold of observed data points for both organs. The simulation reasonably captured the plasma and brain PK of RLZ for the available dosing scenario; however, the model needs to be further evaluated for different dosing scenarios. To the best of our knowledge, no such study in literature was found for rats at a dose other than 10 mg/kg for tablet. Nonetheless, the model provides a starting point for predicting the PK in different dosing scenarios.

Plasma and Brain Concentration for ASD Formulation

The simulated plasma and brain concentration for a single 10 mg/kg ASD formulation of RLZ is shown in Fig. 7 along with the observed data points from our in-house data. For optimization, only plasma concentration was used. The model was reasonably able to capture the brain PK as well.

Fig. 4 *In vitro* dissolution profile of RLZ PAA ASD in the ratio 10:90, 20:80, and 30:70 in comparison with Rilutor **a** at pH 1.2 and **b** in FaSSGF

Fig. 5 Concentration in plasma for Rilutor after 10 mg/kg BW exposure in rat. The blue line, black line, and red line represent the 2.5th percentile, median, and 97.5th percentile, respectively. The observed data from Ravi *et al.*, along with its SD, is represented by red circles [14]
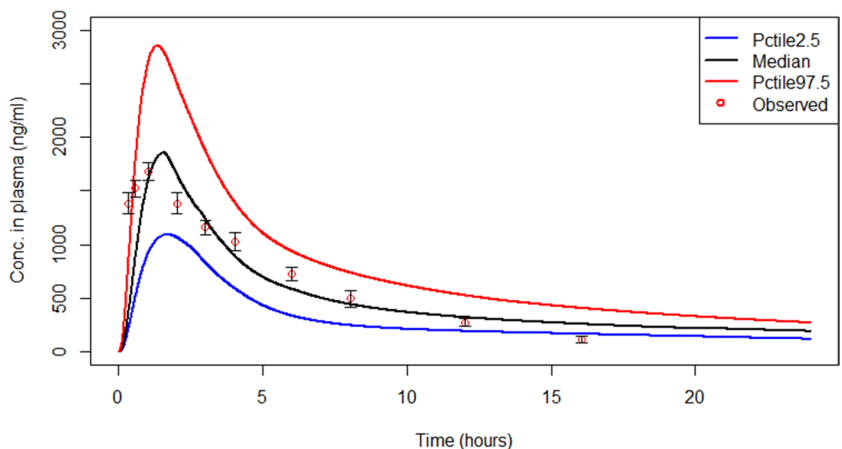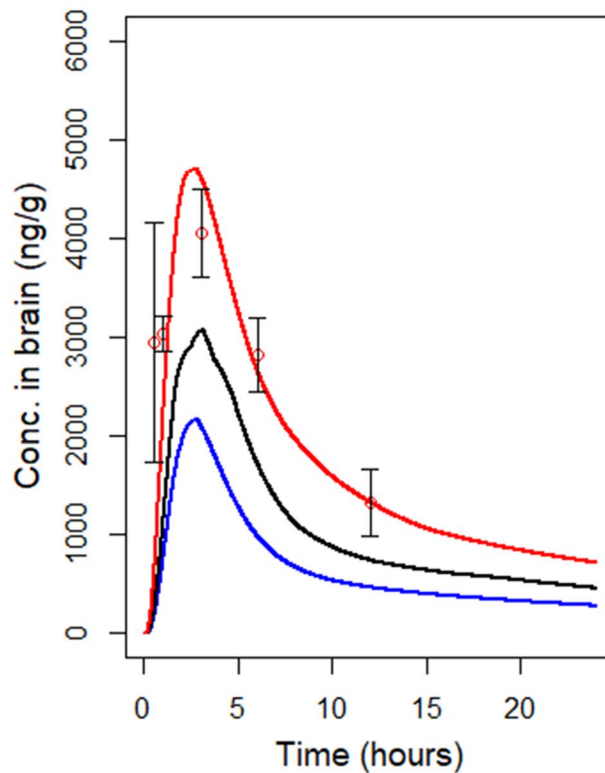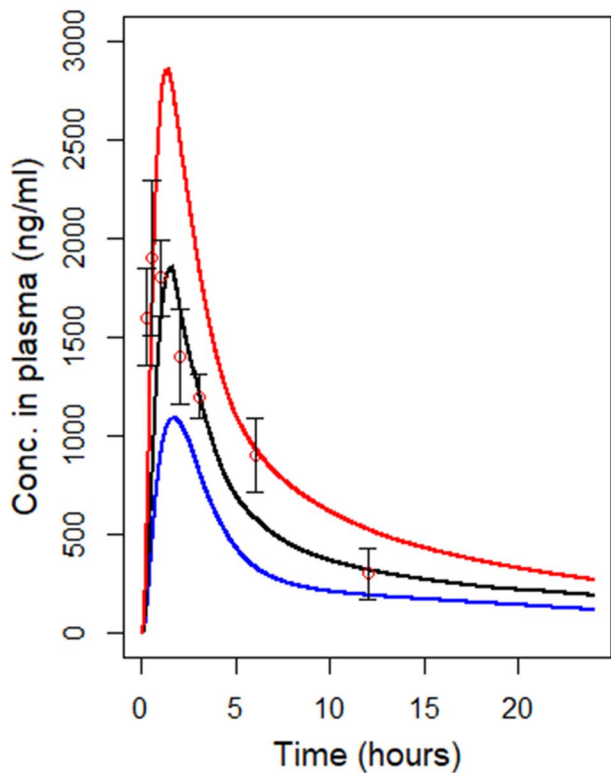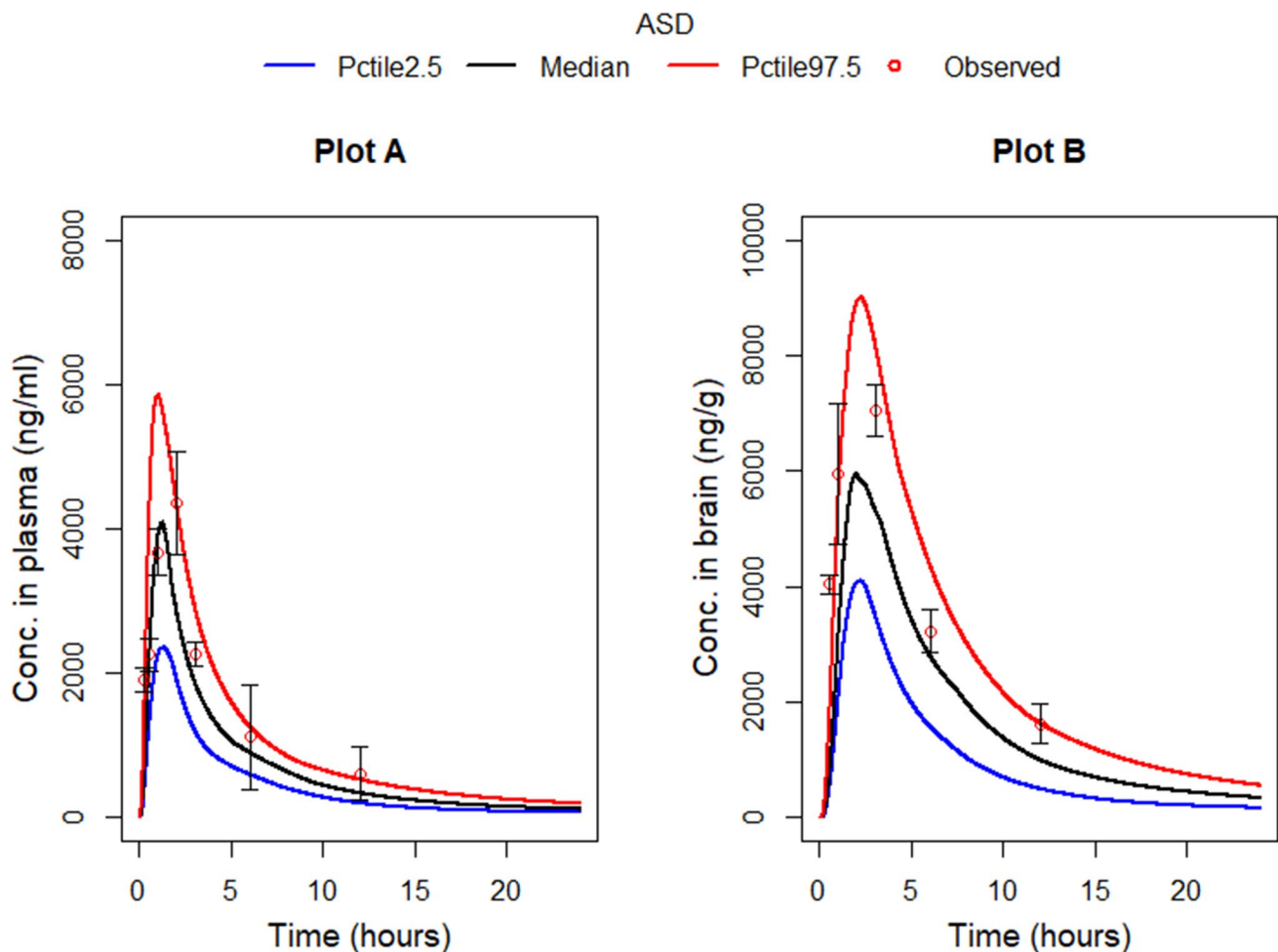

Fig. 6 Concentration-time curve for plasma (Plot A) and brain (Plot B) after dosing of 10 mg/kg BW in rat. The blue line, black line, and red line represent the 2.5th percentile, median, and 97.5th percentile, respectively. The red circles accompanied by bar represent the mean and SD derived from our in-house rat data

Plot A

Plot B

Fig. 7 Concentration-time profile for plasma (Plot A) and brain (Plot B) after dosing of 10 mg/kg BW ASD formulation in rat. The blue line, black line, and red line represent the 2.5th percentile, median, and 97.5th percentile, respectively. The red circles accompanied by bar represent the mean and SD from our in-house rat data

Notably, the simulated and observed C_{max} in brain for ASD (simulated: 5965.075, observed: 7050 ng/g) was 2–3 times higher than Rilutor (Simulated: 3072.61, Observed: 4050 ng/g). AUC was also higher for ASD formulation (simulated brain: 26,532.5, observed brain: 31,700.72 ng/ml * h) compared to Rilutor (simulated brain: 40,044.3, observed brain: 55,093.55 ng/ml * h) in both plasma (Table S2) and brain pointing towards increased efficacy of the formulation.

Human PBPK Model

Concentration-Time Curve for Tablet

The simulated and observed plasma concentrations for a single 50 mg and 100 mg tablet exposure of RLZ are shown in Fig. 8. The simulated C_{max} and AUC were within 2.5 and 97.5 percentiles of the observed data obtained from clinical trials for 50 and 100 mg from Liboux *et al.* [15] and Chandu *et al.* [16]. Increase in the plasma concentration in a dose dependent manner was observed for the Rilutor. As the 50-mg data was not used for optimization, it was used independently for model validation. The model was also able to explain other published data from Longo *et al.* at 50 mg (Figure S2).

In the ASD PBPK, concentration of RLZ in the brain for ASD is higher than the concentration in the brain for Rilutor (Fig. 9). As expected, C_{max} for ASD was about 2–2.5 times higher compared to the tablet, and for the brain AUC as well, a similar trend was observed. This suggests that the overall dosing can be reduced to achieve a similar concentration in the brain as Rilutor, hence reducing the toxicity of RLZ. This can be highly helpful for patients who suffer from RLZ adverse effects due to high-dose administration. In future, this model can be further evaluated with clinical data from ASD formulation.
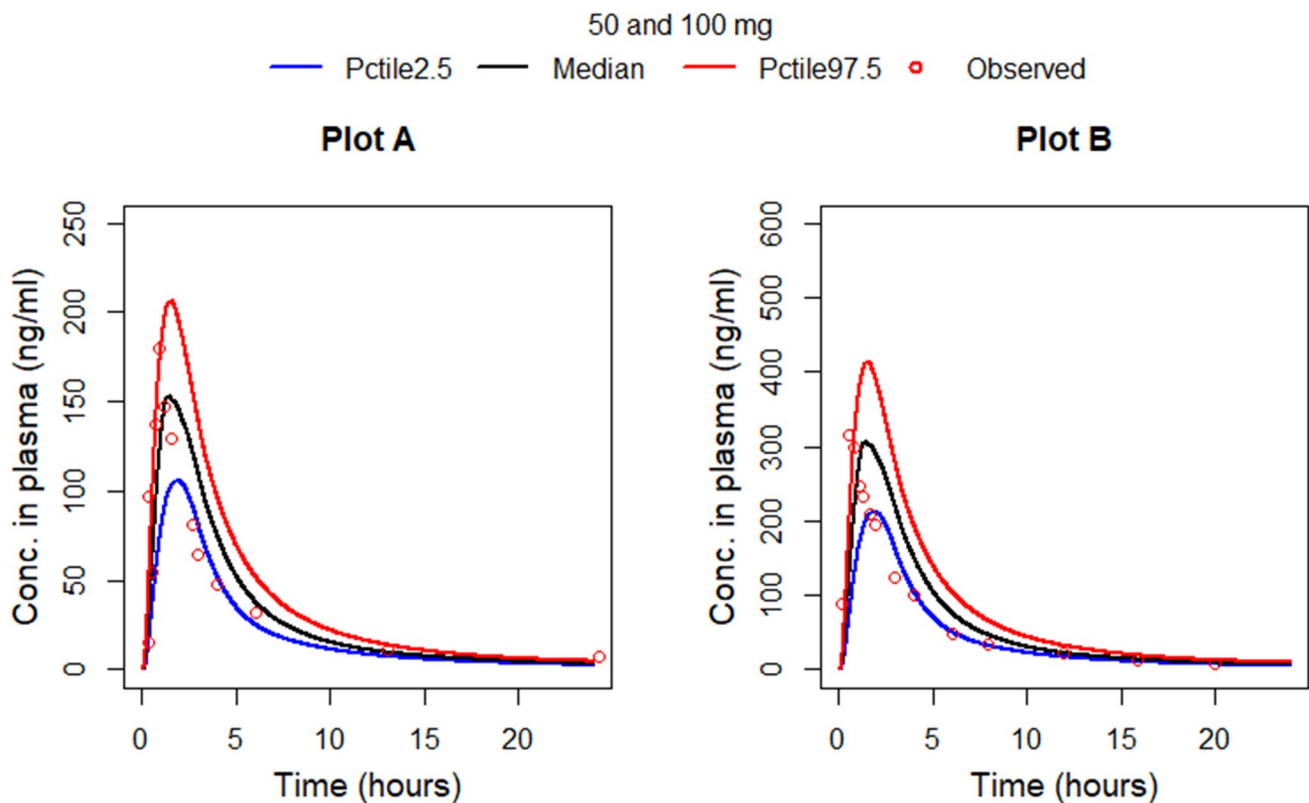
Fig. 8 Concentration-time curve for plasma at the dosing of 50 mg (Plot A) and 100 mg (Plot B). The blue line, black line, and red line represent the 2.5th percentile, median, and 97.5th percentile, respec- tively. Experimental data extracted data from Liboux *et al*. [15] and Chandu *et al*. [16] is represented by red circles

Local Sensitivity Analysis for Rat and Humans

Figure S3 shows local sensitivity analysis for rat PBPK at 10 mg/kg BW tablet. It was found that the rest body: plasma partition coefficient was highly sensitive followed by the liver: plasma partition coefficient, V_{max}, k_m, and fu. In the case of ASD, V_{max} and k_m were highly sensitive towards AUC plasma (Figure S4). This can be due to increased dis- solution and absorption in ASD formulation; as a result, more drug is available in plasma and liver, so metabolic parameters became sensitive due to the limitation of CYP enzymes. This can be one of the reasons for the sensitivity of the liver: plasma partition coefficient. Fu was also sen- sitive, and the rest of other parameters were less than 0.5 (sensitivity coefficient). For the human, Rilutor, and ASD PBPK model, liver: plasma partition coefficient was highly sensitive parameter suggesting that increase in partition coef- ficient will decrease the plasma AUC (Figure S5, S6). This can be possible since more drug present in liver will lead to an increased metabolism and hence reduced AUC in plasma. Fu and V_{max} are also highly sensitive parameter. Another interesting fact is that for human Rilutor, urinary clearance, and fecal elimination were sensitive, whereas they were not so sensitive parameters for ASD formulation.

Discussion

To comprehend the mechanism of drug dissolution and to spot interactions between drug and polymer, solution ^{1}H NMR spectra were used. ^{1}H NMR holds accountability to identify the possible interactions due to any kind of chemical bond formation between drug and polymer. The maximum relative shift in RLZ:PAA could be due to the hydrogen bonding interaction between the NH_2 group of RLZ with the carbonyl oxygen of polymers. The flatness of the dou- blet peak of aromatic hydrogen of RLZ might occur due to C-H···O non-bonding interactions between drug and the polymer or the change in the electron density due to distinct binding interactions between the drug with each polymer [33–35]. The higher order of chemical shift corresponds to the comparatively stronger non-bonding interactions [36]. As the alteration in the chemical shift due to the presence of PAA were more with respect to PVP VA and HPMC AS, it can be inferred that PAA is showing more interactions with RLZ and will stabilize its amorphous state. Similar trend was obtained in contact angle study where PAA in its pure form and in ASD formulation was showing least angle of contact, hence more wettability as compared to other two polymers [37]. PAA has been found to have a direct effect on
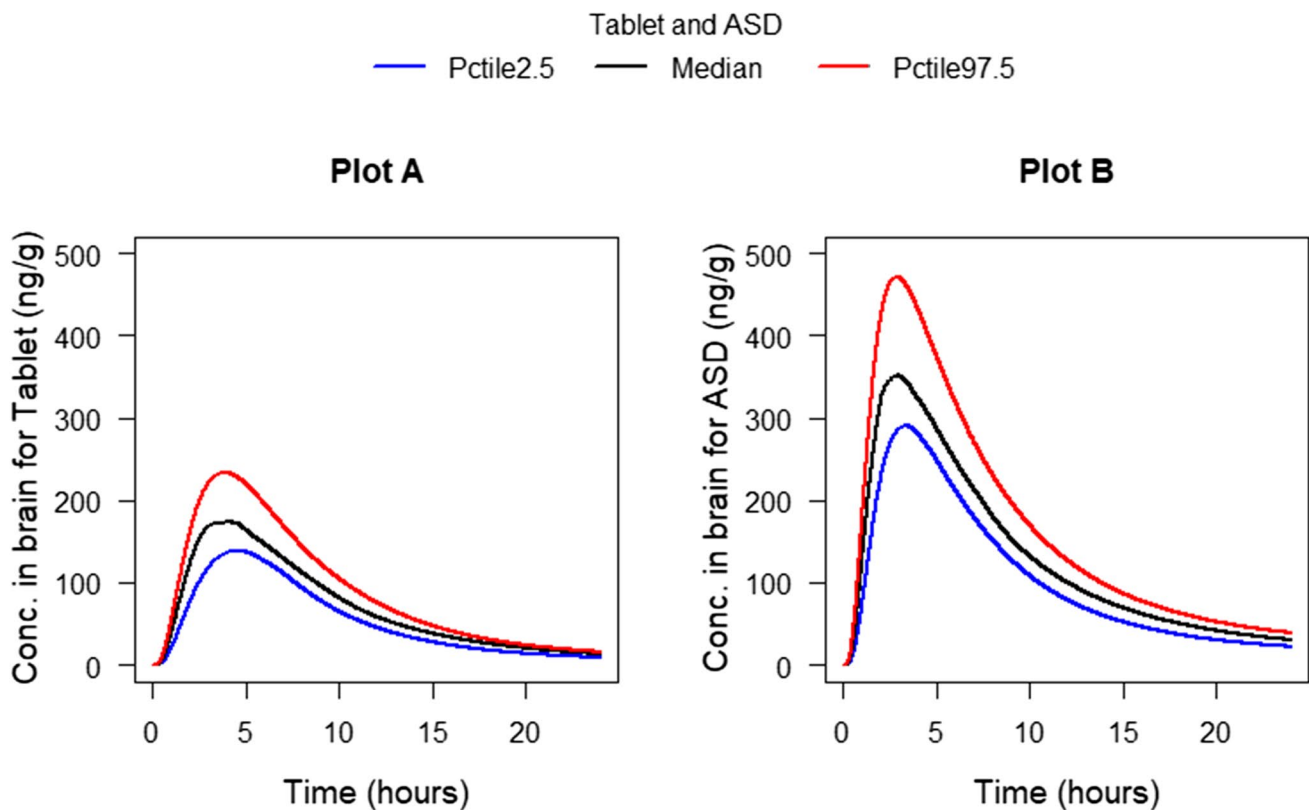
Fig. 9 Concentration-time curve for brain at 50 mg dosing for Rilutor (Plot A) and ASD (Plot B). The blue line, black line, and red line represent the 2.5th percentile, median, and 97.5th percentile, respectively

the hydrophilcity of the formulations [38]. Hence, for further studies, PAA was taken as a polymer of choice and ASDs with different drug:polymer ratios were produced.

In the solid-state characterization, all the three ASD formulations were appearing to be amorphous in nature. In the XRD studies, the broad weak peaks denote the amorphous nature of the prepared ASD in all the ratios. Thus, the XRD study confirms the successful preparation of RLZ ASDs with polymer PAA. In DSC study, no sharp endothermic peaks were observed in any of the ASD formulation confirming complete amorphization of the drug [32]. However, 10:90 RLZ:PAA ASD showed highest change in specific heat indicating more stable amorphous state. In the SAED patterns, the presence of diffused rings and the absence of systematic spots or array indicate the presence of an amorphous solid with complete absence of any crystalline particles. This suggests the formation of ASD with homogenous continuous phase [39, 40].

In the saturation solubility studies, the RLZ solubility at pH 1.2 and FaSSGF was multiple folds higher than its solubility at pH 6.8 and FaSSIF; hence, the *in vitro* dissolution studies at pH 6.8 and FaSSIF was ruled out for further studies. The saturation solubility data is also supported by

Handerson-Haselbalch equation in which pH 1.2 facilitates 99.5% ionization of RLZ while pH 6.8 facilitates only 0.05% ionization [41]. Also, RLZ has an absorption site of upper gastrointestinal tract [42]; hence, dissolution at pH 1.2 and FaSSGF was more relevant. In the dissolution studies, all the formulations showed improved dissolution profile over Rilutor. It was due to the relatively lower solubility of the crystalline RLZ present in Rilutor. All the three ratios of RLZ ASD resulted in substantially enhanced dissolution profile, where10:90 RLZ: PAA ASD had the highest rate of drug release; hence, it was chosen for conducting further studies. The higher rate of drug release in FaSSGF than at pH 1.2 could be due to the surfactants present in the biorelevant media [43, 44]. The enhanced dissolution profile of 10:90 RLZ:PAA ASD over the other ASDs can be explained based on the phenomena of dissolution of ASDs being polymer-controlled at lower drug loadings [45–47]. PAA is a water-soluble polymer [1]; hence, the higher polymer concentration leads to higher drug dissolution. Additionally, water induced amorphous-amorphous phase separation could be a reason of lower drug release with subsequent increase in the drug loading [48]. It is mentioned in other studies as well that PAA which is an anionic polymer shows ionic interactions with

weakly basic drugs which result in a dramatic decrease in molecular mobility and hence decreased crystallization propensity of the drug [49]. In the pharmacokinetic studies, the ASD formulation showed enhanced profile (C_{max} and AUC) as compared to Rilutor owing to the high-energy physical form of RLZ [50].

After successful development and characterization of the formulation, PBPK model was developed for tablet and ASD with oral dosing to simulate the RLZ concentration in different organs with time. The model was parameterized based on species-specific physiological and biochemical data. Partition coefficient was kept same for both the models. Allometric scaling was applied to scale biochemical parameters from rat to human [51, 52]. Parametric uncertainties were included, and multiple iterations were run with Monte Carlo simulation to assess the uncertainty in RLZ concentration in different organs. The model carries the capability to predict both the RLZ and its metabolite RLZ-OH in multiple organs thus enhancing its capacity to predict safety and efficacy in multiple organs. For the sake of simplicity and due to unavailability of data especially V_{max} and k_m, multiple metabolites for the model were not considered. Another aspect worth mentioning is the polymorphic hepatic CYP450 metabolism may lead to more inter-subject variability especially in human [4]. Currently, polymorphism was not considered, but it may lead to some interesting outcomes, for instance, observed hepatotoxicity in specific individuals [53, 54]. Nonetheless, the PBPK model developed here can act as a starting point to explore mechanistic PK for Rilutor and RLZ ASD.

The developed PBPK model predicted fairly well for tablet and ASD formulation in rat; however, the limitation was the unavailability of data at multiple doses. Since a similar dose was used for optimizing 3–4 biochemical parameters, considerable uncertainty exists for the robustness of the PBPK model in rats. Nonetheless, the plasma concentration was used for optimizing the rat model; the model showed good prediction in brain as well without any further optimization. For human Rilutor, the model validity can be confirmed since after optimizing the model at one dose, it performed well for other dosing scenarios (Fig. 8).

The results of this study are promising for PBPK application in dose design especially in the context of target tissue concentration. Interestingly, it was observed that C_{max} for ASD was almost double compared to Rilutor in brain for the rat with similar trend for human. The increased C_{max} for RLZ ASD points towards increased active concentration in brain for ASD hence may result in improved efficacy. The model developed here can be further used to predict the concentration in urine, feces, and also in other organs of human body, thus understanding the toxicity. The current model can also be adapted to large human population by considering the metabolic and genetic diversity which may explain the sensitivity of population towards adverse effects of RLZ.

In future, the developed PBPK model can be extended to include multiple age groups and diseased populations. Further, an *in vitro* study of the phase transformation of the amorphous form to a crystalline form of RLZ could be studied to evaluate its effect at later stages of dissolution as well as its differential absorption due to different solid-state forms of active drug in different parts of the gastrointestinal tract. The phase transformation data would contribute to the development of physiologically based biopharmaceutical (PBBM) modeling with a particular focus on the saturated, supersaturated, dissolved, and undissolved drugs in the gastrointestinal tract [50, 55]. Availability of such experimental data can help in including the biopharmaceutical component, thus strengthening the mechanistic aspect of kinetic model.

Conclusion

In the current study, ASD of RLZ was successfully developed. Characterization studies like PXRD, DSC, and TEM confirmed the formation of ASD with no trace of crystalline drug present in it. *In vitro* and *in vivo* evaluation indicated improved drug dissolution and pharmacokinetic profile. Furthermore, the PBPK model was developed for rat and human simulating the concentration of RLZ in ASD and in Rilutor in organs following an oral dose. The developed model was able to closely predict the concentration-time profile with limited experimental data. Further data availability can help in providing more mechanistic picture about the formulation aspect of modeling. Nonetheless, the developed model can be used for estimating the dosing scenario for the prepared ASD formulation to achieve a similar PK profile as Rilutor along with reduced toxicity. Since ASD formulation provided a promising approach for increased AUC with a similar dose, hence, further toxicity and efficacy can be evaluated in other species before moving to clinical studies.

Declarations

Ethics Approval The ethical approval for conducting animal experiment was taken from the committee (IIT(BHU)/IAEC/2022/010).

Competing Interests The authors declare no competing interests.

References

1. Amponsah-Efah KK, Mistry P, Eisenhart R, Suryanarayanan R. The influence of the strength of drug–polymer interactions on the dissolution of amorphous solid dispersions. Mol Pharm. 2020;18(1):174–86. https://doi.org/10.1021/acs.molpharmaceut.0c00790.

2. Bhujbal SV, Mitra B, Jain U, Gong Y, Agrawal A, Karki S, Taylor LS, Kumar S, Zhou QT. Pharmaceutical amorphous solid dispersion: a review of manufacturing strategies. Acta Pharm Sin B. 2021;11(8):2505–36. https://doi.org/10.1016/j.apsb.2021.05.014.

3. Dhondale MR, Thakor P, Nambiar AG, Singh M, Agrawal AK, Shastri NR, Kumar D. Co-Crystallization approach to enhance the stability of moisture-sensitive drugs. Pharmaceutics. 2023;15(1):189. https://doi.org/10.3390/pharmaceutics15010189.

4. Dash RP, Babu RJ, Srinivas NR. Two decades-long journey from riluzole to edaravone: revisiting the clinical pharmacokinetics of the only two amyotrophic lateral sclerosis therapeutics. Clin Pharmacokinet. 2018;57:1385–98. https://doi.org/10.1007/s40262-018-0655-4.

5. Doble A. The pharmacology and mechanism of action of riluzole. Neurology. 1996;47(6 Suppl 4):233S-S241. https://doi.org/10.1212/WNL.47.6_Suppl_4.233S.

6. Dharmadasa T, Kiernan MC. Riluzole, disease stage and survival in ALS. Lancet Neurol. 2018;17(5):385–6. https://doi.org/10.1016/S1474-4422(18)30091-7.

7. Lacomblez L, Bensimon G, Leigh PN, Debove C, Bejuit R, Truffinet P, Meininger V. Long-term safety of riluzole in amyotrophic lateral sclerosis. Amyotrophic Lateral Sclerosis and Other Motor Neuron Disorders. 2002;3(1):23–9. https://doi.org/10.1080/146608202317576507.

8. Bensimon G, Doble A. The tolerability of riluzole in the treatment of patients with amyotrophic lateral sclerosis. Expert opinion on drug safety. 2004;3(6):525–34. https://doi.org/10.1517/14740338.3.6.525.

9. Brouwers J, Brewster ME, Augustijns P. Supersaturating drug delivery systems: the answer to solubility-limited oral bioavailability? J Pharm Sci. 2009;98(8):2549–72. https://doi.org/10.1002/jps.21650.

10. Tsai YM, Chien CF, Lin LC, Tsai TH. Curcumin and its nanoformulation: the kinetics of tissue distribution and blood–brain barrier penetration. Int J Pharm. 2011;416(1):331–8. https://doi.org/10.1016/j.ijpharm.2011.06.030.

11. Deepika D, Kumar V. The role of "physiologically based pharmacokinetic model (PBPK)" new approach methodology (NAM) in pharmaceuticals and environmental chemical risk assessment. Int J Environ Res Public Health. 2023;20(4):3473. https://doi.org/10.3390/ijerph20043473.

12. Van Kan HJ, Spieksma M, Groeneveld GJ, Toraño JS, Van den Berg LH, Guchelaar HJ. A validated HPLC assay to monitor riluzole plasma or serum concentrations in patients with amyotrophic lateral sclerosis. Biomed Chromatogr. 2004;18(9):723–6. https://doi.org/10.1002/bmc.384.

13. Ravi PR, Vats R, Reddy KU. Validation of a simple, rapid and sensitive LC method for quantification of riluzole in rat plasma and its pharmacokinetic application. J Bioanal Biomed S. 2012;6:2. https://doi.org/10.4172/1948-593X.S6-007.

14. Rohatgi A. WebPlotDigitizer (Version 3.9) [Computer software]. 2015. Available from: https://automeris.io/WebPlotDigitizer.

15. Liboux AL, Lefebvre P, Roux YL, Truffinet P, Aubeneau M, Kirkesseli S, Montay G. Single-and multiple-dose pharmacokinetics of riluzole in white subjects. J Clin Pharmacol. 1997;37(9):820–7. https://doi.org/10.1002/j.1552-4604.1997.tb05630.x.

16. Chandu BR, Nama S, Kanala K, Challa BR, Shaik RP, Khagga M. Quantitative estimation of riluzole in human plasma by LC-ESI-MS/MS and its application to a bioequivalence study. Anal Bioanal Chem. 2010;398:1367–74. https://doi.org/10.1007/s00216-010-4034-8.

17. Longo DM, Shoda LK, Howell BA, Coric V, Berman RM, Qureshi IA. Assessing effects of BHV-0223 40 mg Zydis sublingual formulation and Riluzole 50 mg Oral tablet on liver function test parameters utilizing DILIsym. Toxicol Sci. 2020;175(2):292–300. https://doi.org/10.1093/toxsci/kfaa019.

18. Rodgers T, Rowland M. Physiologically based pharmacokinetic modelling 2: predicting the tissue distribution of acids, very weak bases, neutrals and zwitterions. J Pharm Sci. 2006;95(6):1238–57. https://doi.org/10.1002/jps.20502.

19. Utsey K, Gastonguay MS, Russell S, Freling R, Riggs MM, Elmokadem A. Quantification of the impact of partition coefficient prediction methods on physiologically based pharmacokinetic model output using a standardized tissue composition. Drug Metab Dispos. 2020;48(10):903–16. https://doi.org/10.1124/dmd.120.090498.

20. Wishart DS, Knox C, Guo AC, Shrivastava S, Hassanali M, Stothard P, Chang Z, Woolsey J. DrugBank: a comprehensive resource for in silico drug discovery and exploration. Nucleic Acids Res. 2006;34(Database issue):D668–72. https://doi.org/10.1093/nar/gkj067.

21. Hu ZY, Lu J, Zhao Y. A physiologically based pharmacokinetic model of alvespimycin in mice and extrapolation to rats and humans. Br J Pharmacol. 2014;171(11):2778–89. https://doi.org/10.1111/bph.12609.

22. Campbell JL Jr, Andersen ME, Hinderliter PM, Yi KD, Pastoor TP, Breckenridge CB, Clewell HJ III. PBPK model for atrazine and its chlorotriazine metabolites in rat and human. Toxicol Sci. 2016;150(2):441–53. https://doi.org/10.1093/toxsci/kfw014.

23. Stevens AJ, Campbell Jr JL, Travis KZ, Clewell III HJ, Hinderliter PM, Botham PA, Cook AR, Minnema DJ, Wolf DC. Paraquat pharmacokinetics in primates and extrapolation to humans. Toxicol ApplPharmacol. 2021;417:115463. https://doi.org/10.1016/j.taap.2021.115463.

24. Brown RP, Delp MD, Lindstedt SL, Rhomberg LR, Beliles RP. Physiological parameter values for physiologically based pharmacokinetic models. Toxicol Ind Health. 1997;13(4):407–84. https://doi.org/10.1177/074823379701300401.

25. Emond C, Raymer JH, Studabaker WB, Garner CE, Birnbaum LS. A physiologically based pharmacokinetic model for developmental exposure to BDE-47 in rats. Toxicol Appl Pharmacol. 2010;242(3):290–8. https://doi.org/10.1016/j.taap.2009.10.019.

26. Sharma RP, Kumar V, Schuhmacher M, Kolodkin A, Westerhoff HV. Development and evaluation of a harmonized whole body physiologically based pharmacokinetic (PBPK) model for flutamide in rats and its extrapolation to humans. Environ Res. 2020;182:108948. https://doi.org/10.1016/j.envres.2019.108948.

27. Loccisano AE, Campbell Jr JL, Andersen ME, Clewell III HJ. Evaluation and prediction of pharmacokinetics of PFOA and PFOS in the monkey and human using a PBPK model. Regul Toxicol Pharmacol. 2011;59(1):157–75. https://doi.org/10.1016/j.yrtph.2010.12.004.

28. Shah DK, Betts AM. Towards a platform PBPK model to characterize the plasma and tissue disposition of monoclonal antibodies in preclinical species and human. J Pharmacokinet Pharmacodyn. 2012;39:67–86. https://doi.org/10.1007/s10928-011-9232-2.

29. Davies B, Morris T. Physiological parameters in laboratory animals and humans. Pharm Res. 1993;10(7):1093–5. https://doi.org/10.1023/A:1018943613122.

30. Milane A, Tortolano L, Fernandez C, Bensimon G, Meininger V, Farinotti R. Brain and plasma riluzole pharmacokinetics: effect of minocycline combination. J Pharm Pharm Sci. 2009;12(2):209–17. https://doi.org/10.18433/J36C78.

31. Saboo S, Moseson DE, Kestur US, Taylor LS. Patterns of drug release as a function of drug loading from amorphous solid dispersions: a comparison of five different polymers. Eur J Pharm Sci. 2020;1(155): 105514. https://doi.org/10.1016/j.ejps.2020.105514.

32. Patel RJ, Patel AA, Patel HP. Stabilized amorphous state of riluzole by immersion-rotavapor method with synthesized mesoporous SBA-15 carrier to augment in-vitro dissolution. J Drug Deliv Sci Technol. 2021;61:102270. https://doi.org/10.18433/J36C78.

33. Jasani MS, Kale DP, Singh IP, Bansal AK. Influence of drug–polymer interactions on dissolution of thermodynamically highly unstable cocrystal. Mol Pharm. 2018;16(1):151–64. https://doi.org/10.1021/acs.molpharmaceut.8b00923.

34. Baghel S, Cathcart H, O'Reilly NJ. Understanding the generation and maintenance of supersaturation during the dissolution of amorphous solid dispersions using modulated DSC and 1H NMR. Int J Pharm. 2018;536(1):414–25. https://doi.org/10.1016/j.ijpharm.2017.11.056.

35. Ueda K, Higashi K, Moribe K. Unusual correlation between the apparent amorphous solubility of a drug and solubilizer concentration revealed by NMR analysis. Mol Pharm. 2022;19(9):3336–49. https://doi.org/10.1021/acs.molpharmaceut.2c00478.

36. Abraham RJ, Mobli M. An NMR, IR and theoretical investigation of 1H chemical shifts and hydrogen bonding in phenols. Magn Reson Chem. 2007;45(10):865–77. https://doi.org/10.1002/mrc.2060.

37. Yu D, Fiddler F, Ibrahim A, Sanedrin R, Tremblay H, Hoag SW. Surface characterization as a tool for identifying the factors affecting the dissolution rate of amorphous solid dispersion tablets. AAPS PharmSciTech. 2022;23(8):282. https://doi.org/10.1208/s12249-022-02413-7.

38. Zenoozi S, Sadeghi GM, Rafiee M. Synthesis and characterization of biocompatible semi-interpenetrating polymer networks based on polyurethane and cross-linked poly (acrylic acid). Eur Polymer J. 2020;5(140): 109974. https://doi.org/10.1016/j.eurpolymj.2020.109974.

39. S'ari M, Blade H, Cosgrove S, Drummond-Brydson R, Hondow N, Hughes LP, Brown A. Characterization of amorphous solid dispersions and identification of low levels of crystallinity by transmission electron microscopy. Mol Pharm. 2021;18(5):1905–19. https://doi.org/10.1021/acs.molpharmaceut.0c00918.

40. Marsac PJ, Rumondor AC, Nivens DE, Kestur US, Stanciu L, Taylor LS. Effect of temperature and moisture on the miscibility of amorphous dispersions of felodipine and poly (vinyl pyrrolidone). J Pharm Sci. 2010;99(1):169–85. https://doi.org/10.1002/jps.21809.

41. Narasimham L, Barhate VD. Physico-chemical characterization of some beta blockers and anti-diabetic drugs-potentiometric and spectrophotometric pKa determination in different co-solvents. Eur J Chem. 2011;2(1):36–46. https://doi.org/10.5155/eurjchem.2.1.36-46.371.

42. Fehlings MG, Wilson JR, Frankowski RF, Toups EG, Aarabi B, Harrop JS, Shaffrey CI, Harkema SJ, Guest JD, Tator CH, Burau KD. Riluzole for the treatment of acute traumatic spinal cord injury: rationale for and design of the NACTN Phase I clinical trial. J Neurosurg Spine. 2012;17(Suppl1):151–6. https://doi.org/10.3171/2012.4.AOSPINE1259.

43. Correa-Soto CE, Gao Y, Indulkar AS, Zhang GG, Taylor LS. Role of surfactants in improving release from higher drug loading amorphous solid dispersions. Int J Pharm. 2022;25(625): 122120. https://doi.org/10.1016/j.ijpharm.2022.122120.

44. Mah PT, Peltonen L, Novakovic D, Rades T, Strachan CJ, Laaksonen T. The effect of surfactants on the dissolution behavior of amorphous formulations. Eur J Pharm Biopharm. 2016;1(103):13–22. https://doi.org/10.1016/j.ejpb.2016.03.007.

45. Que C. Optimization of dissolution performance for amorphous solid dispersions. Purdue University Graduate School. Thesis. 2019. https://doi.org/10.25394/PGS.11301389.v1.

46. Indulkar AS, Lou X, Zhang GG, Taylor LS. Insights into the dissolution mechanism of ritonavir–copovidone amorphous solid dispersions: importance of congruent release for enhanced performance. Mol Pharm. 2019;16(3):1327–39. https://doi.org/10.1021/acs.molpharmaceut.8b01261.

47. Saboo S, Mugheirbi NA, Zemlyanov DY, Kestur US, Taylor LS. Congruent release of drug and polymer: a "sweet spot" in the dissolution of amorphous solid dispersions. J Control Release. 2019;28(298):68–82. https://doi.org/10.1016/j.jconrel.2019.01.039.

48. Yang R, Zhang GG, Zemlyanov DY, Purohit HS, Taylor LS. Release mechanisms of amorphous solid dispersions: role of drug-polymer phase separation and morphology. J Pharm Sci. 2023;112(1):304–17. https://doi.org/10.1016/j.xphs.2022.10.021.

49. Mistry P, Mohapatra S, Gopinath T, Vogt FG, Suryanarayanan R. Role of the strength of drug–polymer interactions on the molecular mobility and crystallization inhibition in ketoconazole solid dispersions. Mol Pharm. 2015;12(9):3339–50. https://doi.org/10.1021/acs.molpharmaceut.5b00333.

50. Thakore SD, Thakur PS, Shete G, Gangwal R, Narang AS, Sangamwar AT, Bansal AK. Assessment of biopharmaceutical performance of supersaturating formulations of carbamazepine in rats using physiologically based pharmacokinetic modeling. AAPS PharmSciTech. 2019;20:1–2. https://doi.org/10.1208/s12249-019-1386-z.

51. Deepika D, Sharma RP, Schuhmacher M, Kumar V. Risk assessment of perfluorooctane sulfonate (PFOS) using dynamic age dependent physiologically based pharmacokinetic model (PBPK) across human lifetime. Environ Res. 2021;1(199): 111287. https://doi.org/10.1016/j.envres.2021.111287.

52. Choi GW, Lee YB, Cho HY. Interpretation of non-clinical data for prediction of human pharmacokinetic parameters: in vitro-in vivo extrapolation and allometric scaling. Pharmaceutics. 2019;11(4):168. https://doi.org/10.3390/pharmaceutics11040168.

53. Remy AJ, Camu W, Ramos J, Blanc P, Larrey D. Acute hepatitis after riluzole administration. J Hepatol. 1999;30(3):527–30. https://doi.org/10.1016/S0168-8278(99)80115-9.

54. Sheng YJ, Wu G, He HY, Chen W, Zou YS, Li Q, Zhong L, Huang YM, Deng CL. The association between CYP2E1 polymorphisms and hepatotoxicity due to anti-tuberculosis drugs: a meta-analysis. Infect Genet Evol. 2014;1(24):34–40. https://doi.org/10.1016/j.meegid.2014.01.034.

55. Purohit HS, Trasi NS, Sun DD, Chow EC, Wen H, Zhang X, Gao Y, Taylor LS. Investigating the impact of drug crystallinity in amorphous tacrolimus capsules on pharmacokinetics and bioequivalence using discriminatory in vitro dissolution testing and physiologically based pharmacokinetic modeling and simulation. J Pharm Sci. 2018;107(5):1330–41. https://doi.org/10.1016/j.xphs.2017.12.024.